Supplementary Information for
Multiscale Insights into Sodium Storage in Hard Carbon from Operando Small- and Wide-Angle Neutron Scattering Measurements

-Angle Battery Cell

Figures S1(a) and 1(b) present a 3D rendering of the custom-designed operando electrochemical cell and its photograph. The cell adopts a three-electrode configuration comprising working, reference, and counter electrodes. The top, middle, and bottom components are made of aluminum, and a Cd mask with an aperture of 8 or 10 mm is positioned beneath the top section to define the neutron beam. Neutron-transparent Cu or Al windows are mounted on the inner sides of the top and bottom sections and also serve as current collectors, enabling direct analysis of the electrode materials. Two integrated springs are incorporated to improve electrical contact with the current collector windows. The cell supports both transmission and reflection geometries and is compatible with the wide-angle detector banks of the TAIKAN instrument. The angular aperture is designed to be 110° on both sides, enabling a broad q-range to be covered in a single measurement.

More detailed information about this cell is described in Ref. [S1].

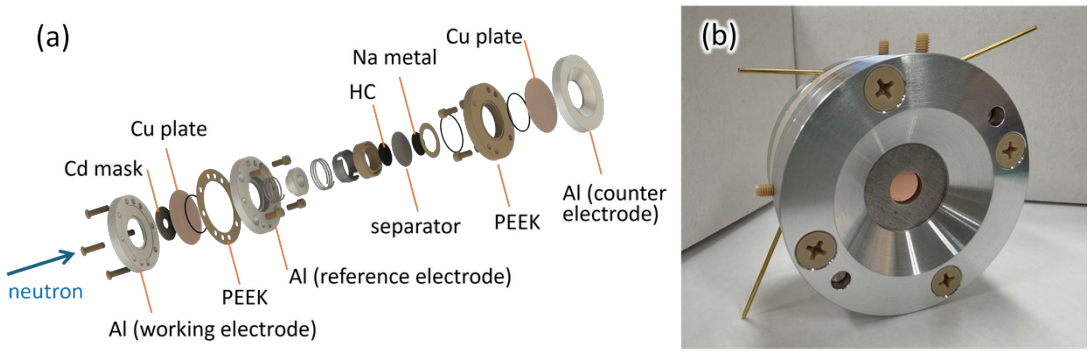

Figure S1. (a) Schematic of the operando cell. (b) Photograph of the developed operando cell for SANS and WANS experiment.

2 SANS Region Analysis Model

We employed Eq. (S1) to describe the broad hump observed in the SANS profiles. The details of the parameter a_0 are described in Section 2.1, and the differences between

the present model and those used in previous operando SANS study (Ref. [S2]) are discussed in Section 2.2.

$$I(Q) = \frac{I_{nanopore}}{1 + 2a_0^2Q^2 + a_0^4Q^4} \quad Eq.\ (S1)$$

2.1 Assumption of Volume Invariance in the Nanopore Region and Definition of a_0

The analysis of the SANS intensity variations (Eq. (5) at main text) relies critically on the assumptions that the volume fractions of the two phases remain constant and that the electrolyte does not penetrate the carbon matrix. In the following, we discuss the validity of this assumption and examine how allowing the nanopore volume to vary (i.e., treating a_0 as a variable) affects the analysis results and their implications for the discussion of $I_{nanopore}$.

We consider it reasonable to assume that the volume of the nanopore region in hard carbon remains essentially constant during charging. The average nanopore radius is $R = a_0\sqrt{10} \approx 1$nm, whereas the typical ionic radius of Na^+ is approximately 0.1 nm. Assuming spherical nanopores, the pore volume is roughly 10^3 times larger than that of a single Na^+ ion, indicating that Na^+ insertion is unlikely to induce significant distortion or collapse of the carbon framework. Moreover, although expansion of graphene-like layers upon Na^+ insertion could exert some stress on the surrounding structure, the much lower density of hard carbon compared to graphite suggests that changes in the interlayer spacing of graphene-like domains have minimal impact on the nanopore volume. Furthermore, the experimental observation that almost no cracks formed in the relatively less plastic NASICON phase after long-term cycling in carbon/NASICON composite electrodes (Ref. [S3]) supports the volume-invariant assumption. Therefore, the nanopore volume can be regarded as effectively constant, justifying the volume-invariant nanopore assumption.

Regarding the assumption of negligible electrolyte penetration into the carbon matrix, Hasegawa *et al.* (Ref. [S4]) provide supporting experimental evidence. Helium (He) pycnometry measurements indicate the formation of nanostructures inaccessible to He atoms. Given that solvated Na^+ ions and counter anions are substantially larger than He,

it is highly unlikely that they can penetrate nanopores that are inaccessible to He. This supports the assumption that electrolyte penetration into the nanopore region is negligible.

We now address the apparent discrepancy between our results and those reported in the prior operando SANS study by Reynolds *et al.* (Ref. [S2]). This discrepancy does not stem from differences in material properties; both studies used commercially available industrial hard carbons with broadly similar manufacturer-reported physical properties (Table 1). The overall features of the operando SANS profiles are also consistent. Minor differences in experimental conditions, such as the charging time to reach the fully charged state, exist; however, the observed discrepancy primarily arises from differences in data interpretation. Reynolds *et al.* incorporated volume changes estimated from dilatometry, assuming different expansion ratios for the slope and plateau regions, whereas we adopted the conclusion of Ref. [S2] that hard carbon exhibits negligible volume change during charging. Recalculating the SLD from Reynolds *et al.*'s data under a constant density assumption yields a monotonic decrease consistent with the trend in our normalized SANS intensity (Fig. 4(c) at main text), confirming that the difference is largely analytical rather than intrinsic.

Table1: HC Properties

	Carbotron (J), (Kureha Co., Ltd.)	Kuranode Type I, (Kuraray Co., Ltd.)
Average Particle size (μm)	9	9
Specific Surface Area (m^2/g)	3~7	4
Interlayer spacing (nm)	0.37~0.38	0.38

Finally, we examined the effect of treating a_0 as a free parameter. As shown in **Fig. S2**, allowing a_0 to vary does not change the overall trend of $I_{nanopore}$. In our model,

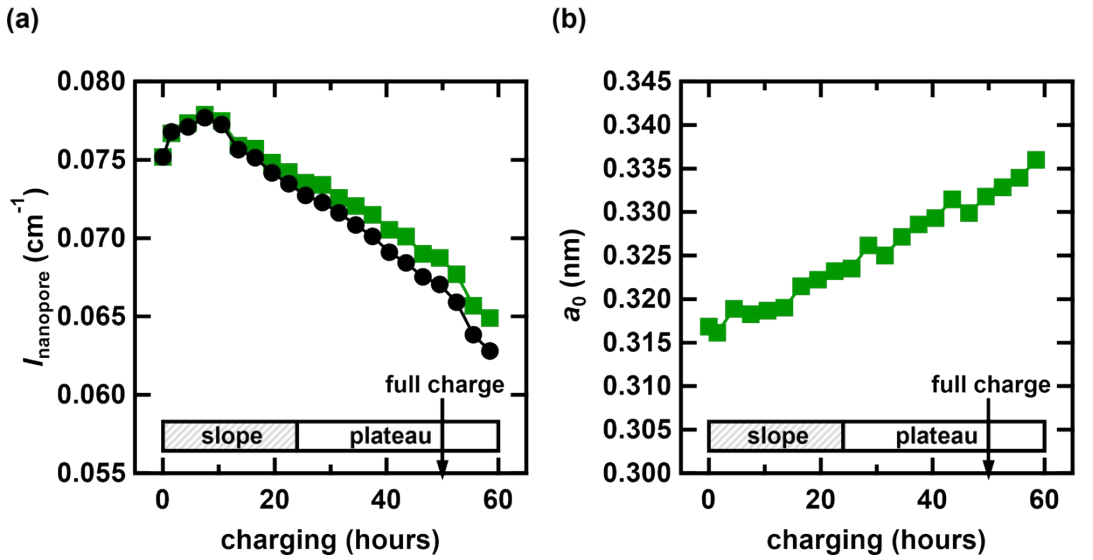

Figure S2. Initial charge-time dependence of the analysis parameters: (a) intensity of the nanopore contribution, I_{nanopore}, and (b) pore-size parameter a_0. Black circles represent the fitting results obtained with a_0 fixed, while green squares represent those obtained with a_0 treated as a free parameter.

$I_{nanopore} = Ca_0$, where C is a scale factor. Therefore, variations in a_0 only induce minor quantitative changes in the decreasing rate of $I_{nanopore}$, while the qualitative behavior remains unchanged. This confirms that our main conclusions are robust with respect to the treatment of a_0.

2.2 Justification for the Debye–Bueche Model in SANS Analysis

The broad hump observed in the SANS profiles can be described either by the Debye–Bueche model [Eq. (S1)] or by the Teubner–Strey model [Eq. (S2)].

$$I(Q) = \frac{I_{nanopore}}{1 + C_1 Q^2 + C_2 Q^4} \quad Eq.\ (S2)$$

In the Teubner–Strey model, the pore–pore distance l and the correlation length ξ are derived from the fitting parameters C_1 and C_2, as defined in Eq. (S3a) (S3b).

$$l = \frac{2\pi}{\sqrt{\frac{1}{2\sqrt{C_2}} - \frac{C_1}{4C_2}}} \quad \text{Eq. (S3a)}$$

$$\xi = \frac{2\pi}{\sqrt{\frac{1}{2\sqrt{C_2}} + \frac{C_1}{4C_2}}} \quad \text{Eq. (S3b)}$$

We attempted to analyze our SANS data using the Teubner–Strey model. As shown in **Fig. S3**(a), the numerical fitting converged, yielding $C_1 = 0.207(17)$ and $C_2 = 0.0093(2)$. However, when these values are substituted into Eq. (3a), the numerator approaches zero, causing the pore–pore distance l to diverge. **Figure S3**(b) illustrates this behavior, demonstrating that for certain combinations of C_1 and C_2, in particular, when C_2 is sufficiently small relative to C_1, the pore-pore distance diverges to infinity.

A comparison of Eqs. (S1) and (S2) shows that the Debye–Bueche model corresponds to the limiting case of the Teubner–Strey model, where $C_1 = 2a_0^2$ and $C_2 = a_0^4$. Under this condition, $C_2 = C_1^2/4$, and the pore–pore distance formally becomes infinite. Thus, the Debye–Bueche model can be regarded as the dilute-limit case of the Teubner–Strey model. As illustrated in **Fig. S3**(b), for smaller values of C_1, the range of C_2 values that

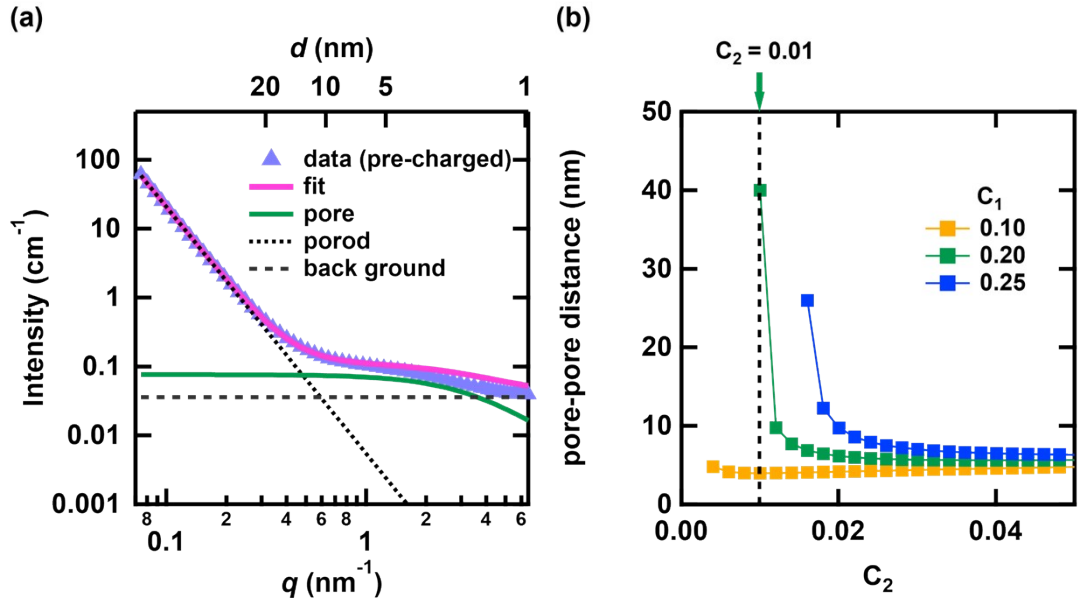

Figure S3. (a) Teubner–Strey model fitting result of the pre-charged SANS profile (solid pink line). The dotted line corresponds to the porod component, the solid green line corresponds to the hump component, and the dashed line corresponds to the background. (b) Calculated pore–pore distance as a function of C_2 for representative C_1 values.

suppress to divergence of l becomes broader. The validity of the obtained C_1 value can be independently assessed. Because the same sample and the same scattering profile are analyzed, if the relation $C_1 = 2a_0^2$ holds, then for the profile before charging with $a_0 = 0.3161(5)$, one obtains $C_1 = 0.1998(3)$. This value is consistent with the fitted value $C_1 = 0.207(17)$, supporting the physical validity of the fitting. The corresponding average nanopore radius, $R \approx 1$ nm, is also a typical value for hard carbon.

We now comment on the differences to the prior operando SANS study by Reynolds *et al.* (Ref. [S2]). For clarity, the analytical parameters reported in Ref. [S2] were converted to consistent units (nm). In Ref. [S2], analysis of SAXS data yielded $a_0 = 0.366$, corresponding to an average nanopore radius of 1.16 nm, which is a typical value for hard carbon. Assuming the relation $C_1 = 2a_0^2$, this gives $C_1 = 0.2679$, which is comparable to the value obtained in the present study. Given that both studies investigated commercially available hard carbons with similar reported physical properties (Table 1), the characteristic structural length scales extracted from the two analyses are broadly consistent.

In their SANS analysis, Ref. [S2] fixed the parameter $C_1 = 0.1055$ and treated only C_2 as a variable parameter. This modeling choice leads to finite values of the pore-pore distance. In the present work, we did not impose such a constraint and instead examined the behavior of the Teubner–Strey parameters without fixing C_1. As a result, we found that the pore–pore distance diverges, indicating a dilute-pore regime in which the Debye–Bueche model provides a more appropriate physical description.

We note that these differences primarily reflect distinct analytical strategies rather than contradictions in the experimental observations. The present analysis emphasizes that, for SANS profiles lacking a clear shoulder feature, the Debye–Bueche model offers a physically reasonable limiting description, whereas the Teubner–Strey model may be more suitable for systems with stronger structural correlations.

References

[S1] K. Ohishi, D. Igarashi, R. Terata, K. Nakemoto, Y. Kawamura, M. Toshiaki, K. Hiroi, S. Takata and S. Komaba, *Accepted in JPS Conf. Proc.*, 2025, -, –.

[S2] E. M. Reynolds, J. Fitzpatrick, M. O. Jones, N. Tapia-Ruiz, H. Y. Playford, S. Hull, I. McClelland, P. J. Baker, S. A. Cussen and G. E. Pérez, *J. Mater. Chem. A*, 2024, 12, 18469–18475.

[S3] G. Hasegawa, M. Hattori, K. Nakanishi and K. Hayashi, *Energy Storage Mater.,* 2025, 80, 104437.

[S4] G. Hasegawa, K. Kanamori, N. Kannari, J. ichi Ozaki, K. Nakanishi and T. Abe, *J. Power Sources,* 2016, 318, 41–48.